JASA EXPRESS LETTERS ARTICLE asa.scitation.org/journal/jel

Spatial observations of low-frequency acoustic propagation near isolated seamounts using an autonomous surface vehicle

Matthew McKinley,[1,a] Davis Rider,[1] Laurent Grare,[2] Ganesh Gopalakrishnan,[2] Luc Lenain,[2] and Karim G. Sabra[1]

[1]*School of Mechanical Engineering, Georgia Institute of Technology, Atlanta, Georgia 30332, USA*
[2]*Scripps Institution of Oceanography, University of California San Diego, La Jolla, California 92093, USA*

mmckinley31@gatech.edu, drider3@gatech.edu, lgrare@ucsd.edu, ganeshgopal@ucsd.edu, llenain@ucsd.edu, karim.sabra@me.gatech.edu

Abstract: This work demonstrates the feasibility of using autonomous surface vehicles equipped with a shallow towed acoustic module (TAM) to survey the spatial variability of low-frequency acoustic propagation across complex bathymetry, such as the Atlantis II seamounts in the Northwest Atlantic. The abrupt seamount topography is found to significantly influence the TAM's recordings of chirp transmissions (500–600 Hz band) from a bottom-moored source ∼30 km from the seamounts by notably causing blockage of in-plane propagation paths and complex reverberation arrivals displaying three-dimensional effects, as confirmed by synthetic aperture beamforming. Ray tracing simulations are compared to these observations based on a data-assimilated ocean model.

[Editor: David R. Barclay] https://doi.org/10.1121/10.0036447

Received: 24 December 2024 **Accepted:** 2 April 2025 **Published Online:** 17 April 2025

1. Introduction

Deepwater abrupt topography changes, such as canyons and seamounts, can significantly enhance the complexity of underwater sound propagation by notably creating highly variable three-dimensional (3D) scattering effects (Heaney and Baggeroer, 2006; Ballard and Sagers, 2019; Ballard *et al.*, 2023; Guo *et al.*, 2023), thus making it more challenging to predict numerically (Jensen *et al.*, 2011). Previous numerical studies have used idealized seamount shapes to investigate such effects (Luo and Schmidt, 2009; Lin *et al.*, 2013; Mallik *et al.*, 2024) and more realistic modeled bathymetry near an island (Lin *et al.*, 2022). However, further modeling and experimental studies are needed to investigate the complex sound propagation effects caused by abrupt seamount topography specifically. One avenue to precisely survey the spatial variability of deepwater sound propagation induced by isolated seamounts, e.g., causing topography-induced scattering effects, is to use instrumented autonomous surface vehicles (ASVs) that can be accurately geo-located. These precise acoustic observations can, in turn, be used to validate numerical model predictions in these complex environments.

In 2023–2024, the Office of Naval Research (ONR) sponsored a series of experiments near the Atlantis II (A2) seamounts, which are part of the volcanically created New England Seamount chain. The A2 seamounts were chosen as the study area due to their unique characteristics, comprising three nearby peaks rising more than 3000 m above the seafloor with steep flanks. The central peak on the northern end is traditionally called the A2 summit [A2 label on Fig. 1(a)]. In contrast, the smaller peak to the southeast is called the Caldera [C label on Fig. 1(a)] because it has the typical features of a collapsed volcano. The Gulf Stream (GS) axis frequently crosses over the A2 seamounts' area. Interaction of the GS with the complex bathymetry leads to substantial spatial and temporal sound speed variability near its frontal structure [see Figs. 1(b) and 1(c)] (Godin *et al.*, 2024; McKinley *et al.*, 2024; Walters *et al.*, 2024). While the presence of strong currents in the upper ocean (such as the GS) can create significant operational challenges for ASVs due to set and drift, especially when equipped with a towed array (Premus *et al.*, 2022; Treloar *et al.*, 2024), we demonstrate here the feasibility of using an ASV, specifically an instrumented Liquid Robotics (Herndon, VA) SV3 wave glider (WG) (Grare *et al.*, 2021), to experimentally characterize the spatial variability of low-frequency sound propagation near the A2 seamounts.

To do so, the ASV was equipped with a hydrodynamic towed acoustic module (TAM), composed of a compact tetrahedral hydrophone array (with 13 in. arm length) to minimize drag effect, and a conductivity-temperature-depth (CTD) probe was deployed shallow (depth ∼12 m) along the GS boundary and crossed over the A2 seamounts' region.

[a]Author to whom correspondence should be addressed.

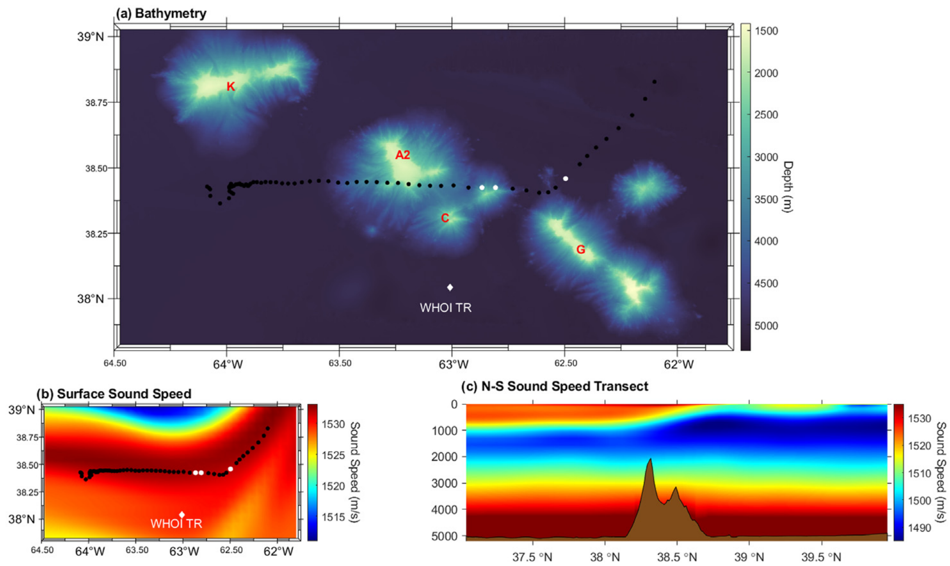

Fig. 1. Wave glider (WG) track at the start of each WHOI-TR transmission cycle (black and white dots) overlayed on bathymetry (a) and simulated surface sound speed (b). White dots represent WG locations where acoustic data are missing. (c) Simulated speed profile South to North transect, which intersects with the Woods Hole Oceanographic Institution Transceiver (WHOI-TR) source (white diamond) at 63.0085°W. K, A2, and G are the Kelvin, Atlantis II, and Gosnold seamounts, respectively, and C is a caldera associated with the Atlantis II seamount complex.

Specifically, the TAM recorded low-frequency chirp transmissions (500–600 Hz) from a bottom-moored source (depth ∼1250 m) located ∼30 km south of the A2 Caldera [see Fig. 1(a)]. We report observations of convergence zone (CZ) propagation paths in the plains surrounding and between A2 seamounts, as well as blockage of the main propagation paths while the WG crosses north of the Caldera, as well as the presence of a complex reverberation arrival structure and 3D (i.e., out of plane) sound propagation effects at most surveyed locations. The out-of-plane propagation effects are confirmed by the synthetic horizontal aperture beamforming of groups of closely spaced successive source transmissions recorded by the WG's TAM. Furthermore, two-dimensional (2D) and 3D ray tracing simulations are performed with input sound speed fields computed from the outputs of a data-assimilated Massachusetts Institute of Technology general circulation model (MITgcm) (Marshall *et al.*, 1997) to help interpret these experimental observations.

2. Methods

2.1 Data collection

Oceanographic and acoustic data were collected using the WG and ASV. The system comprises three components: the surface float (housing the scientific payload, including sensors for conductivity, temperature, and sound velocity), the propulsion unit, called the sub (8 m below the float), and the TAM, positioned at 10–12 m deep, towed ∼10 m behind the sub. The TAM includes a tetrahedral hydrophone array (HTI-96-MIN; High Tech, Inc., Long Beach, MS), a four-channel acoustic recorder (RESEA; RTsys, Caudan, France), and an AML-3 XC probe (AML Oceangraphic, Inc., Victoria, BC, Canada) for measuring CTD parameters and sound velocity. This study used data from a single hydrophone sampled at 39 kHz. The WG was operated along the southern edge of the GS from May 31 to June 2, 2023 [see Fig. 1(a)], during the NESMA-Pilot cruise.

2.2 Passive synthetic array beamforming procedure

The bottom-moored acoustic source [Woods Hole Oceanographic Institution Transceiver (WHOI-TR)] used in this study was deployed at (38.04175°N, 63.0085°W). Initially set at 700 m depth, the source was blown down to 1200–1250 m due to strong local currents while the WG was deployed. Thus, a nominal source depth of 1250 m was used for the acoustic simulations. The source signal was a 2.5-s up-chirp (500–600 Hz), transmitted every 10 s during 5-min intervals at the start of each hour, totaling 30 chirps per hourly cycle. The recording of these successive 30 chirp transmissions by the moving TAM's hydrophone (see Fig. S2 in the supplementary material) enables the emulation of WHOI-TR reception by a 30-element horizontal synthetic array (Autrey, 1988) along the WG's track (see Figs. S2–S6 in the supplementary material). This synthetic array allowed for (1) incoherent stacking of the envelope of the selected arrival windows across the 30 elements of the synthetic aperture to enhance the signal-to-noise ratio of the selected arrival and (2) determining the direction of arrival of the selected arrival window based on incoherent time-delay beamforming (Johnson and Dudgeon, 1993).

The heading of the synthetic array was determined based on the initial geo-localized position of WG's surface float at the start of the 5-min reception period. The standard deviation and mean value of this heading angle over the 5-min reception period are provided in Sec. 3 hereafter. The following simplifying assumptions were also made: (1) The WG has a uniform linear motion for 5 min (or shorter if the time is truncated due to the WG turning significantly between intervals). (2) There is a constant relative position of the TAM to the WG's surface float. (3) There is steady hydrophone depth. (4) The plane wave beamforming procedure used the TAM's average AML-measured mean sound speed over the 5-min reception period. Based on this simple approach and inherent uncertainties, it was found that performing incoherent stacking and beamforming of the selected arrival wavefronts from WHOI-TR transmissions yielded the most robust estimation of their apparent angle of arrival in this complex environment.

2.3 Ocean circulation model setup

The data-assimilated MITgcm solutions provided the sound speed field used for ray tracing simulations. This model solves the Boussinesq equations of motion on a rotating sphere and is implemented on a 1/12° grid (∼9 km resolution) with 50 vertical z-levels and bathymetry from ETOPO-1. Initial and open boundary conditions were derived from HYCOM-GOFS 3.1 1/12° global analysis (Chassignet *et al.*, 2007) and adjusted with Copernicus Marine Environment Monitoring Service (CMEMS) sea surface height (SSH) data. Atmospheric forcing was based on ERA5 reanalysis, and assimilated observations included satellite along-track SSH from Jason-3, CryoSat-2, SARAL/AltiKA, and Sentinel-3A satellites via the Radar Altimeter Database System (RADS) (National Oceanic and Atmospheric Administration, 2024a) and geo-polar daily blended sea surface temperature (SST) data at 5 km resolution (National Oceanic and Atmospheric Administration, 2024b). A four-dimensional variational assimilation (4D-Var) framework (Stammer *et al.*, 2002; Forget *et al.*, 2015) constrained the model state during the selected observation period to enhance the accuracy of the estimates' GS features like eddies and meanders.

2.4 Ray tracing simulations

Ray tracing simulations used BELLHOP (Porter, 2011) and BELLHOP3D (Porter, 2019). The input sound speed field, derived from MITgcm outputs for June 1, 2023, at 12:30, was calculated using the TEOS-10 toolbox (Roquet *et al.*, 2015) and interpolated from a 9 km model resolution to a 1 km resolution. Bathymetry was based on the GEBCO database, while the seafloor was crudely modeled as a fluid layer with a sound speed ratio of 1.5 and attenuation of 0.2 dB/wavelength. Transmission loss (TL) simulations were conducted at the center frequency (550 Hz) of the WHOI-TR transmissions.

3. Results

The ASV was primarily located along the southern edge of the GS, i.e., in the Sargasso Sea [see Figs. 1(a) and 1(b)]. During at-sea operations, this track was selected to ensure the ASV did not experience the full strength of the GS's current to maintain maneuverability. Preliminary comparisons between the physical observations collected by the ASV (i.e., local ocean temperature, salinity, and sound speed) and the outputs of the numerical models are presented in Fig. S1 in the supplementary material. Overall, these comparisons highlight the challenges to accurately predict the details of the meso(sub)-mesoscale GS dynamics, especially at shallow depths [∼12 m here corresponding to the average TAM's depth during the WG deployment; see Fig. S1(d)], with currently available approaches for ocean circulation models. A more detailed analysis will be the scope of future work. In the remainder of the analysis, we will solely focus on the influence of the A2 seamounts' topography on the spatial variability of the recorded low-frequency transmissions from the WHOI-TR source.

Figure 2 shows the predicted TL values (for the center frequency 550 Hz of the WHOI-TR transmissions) at the TAM's depth (12 m) using either 2D [Fig. 2(a)] or 3D [Fig. 2(b)] ray tracing simulations. A notable feature is the typical deepwater CZ propagation ring (at a range of ∼58 km for the first CZ annulus), which is interrupted by the presence of the A2 seamounts. Note that the 3D ray simulations predict a stronger increase in TL behind the seamounts than 2D ray simulations, thus confirming the 3D influence of the seamounts on the blockage of propagation paths originating from WHOI-TR. The ASV's track is also overlaid on Figs. 2(a) and 2(b), with green dots indicating locations where the TAM's hydrophone successfully recorded clear arrivals resulting from WHOI-TR transmissions. In contrast, red dots indicate locations where no clear arrivals were detected on the TAM (see Fig. S5). White dots mark locations where acoustic data were missing due to hardware issues. These observations are consistent with the predicted TL values, confirming that WHOI-TR transmissions can be recorded along most of the ASV's track, except when the ASV was located north of the Caldera [see Fig. 1(a)]. To further illustrate this effect, Fig. 2(c) shows a vertical transect of the TL variations (from 2D ray tracing), which displays the formation of the first CZ and how it can be recorded at the selected shallow TAM's location. On the other hand, Figs. 2(d) and 2(e) show vertical transects of the TL variations, which shows the Caldera seamount can block the WHOI-TR transmissions from reaching the location of the TAM at the selected range. A white vertical line marks the corresponding ASV's range on each transect.

Figure 3 shows examples of the incoherently stacked envelopes of the 30 recorded WHOI-TR transmissions by the TAMs (which were time-aligned based on the delay of the first arrival) for the hours when the ASV crossed near the CZ annulus locations on the western [Fig. 3(b)] or the eastern [Fig. 3(e)] side and also for the hour right before or after

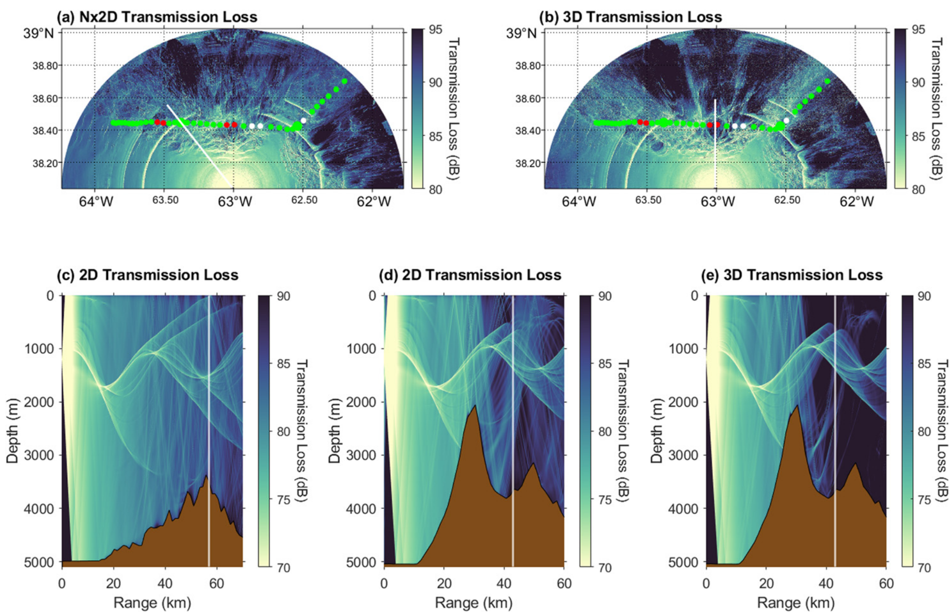

Fig. 2. Nx2D (a) and 3D (b) ray tracing TL simulations at a depth of 12 m overlayed with the WG track. Green dots indicate locations where the WG TAM's hydrophone recorded a clear reception of the WHOI-TR transmissions, while red dots indicate locations where no clear reception was made. White dots indicate locations where acoustic data were missing. Panels (c) and (d) are 2D variations of simulated TL for the transects marked by white lines in panels (a) and (b), respectively. The 3D variation of panel (d) is shown in panel (e).

the CZ crossing [Figs. 3(a), 3(c), and 3(d)]. Each panel first displays a couple of distinct arrivals associated with isolated ray arrivals, followed by a more diffuse sequence of weaker multipath arrivals and reverberation patterns. The amplitude scale is truncated to the same arbitrary threshold on all panels of Figs. 3(a)–3(e) to help visualize the weaker reverberation arrival structure. However, Figs. 3(f) and 3(g) display the full amplitude scale of the CZ receptions (see gray and red shaded arrivals) recorded, respectively, on the western side or the eastern side of the A2 seamounts [same as Figs. 3(b) and 3(e), respectively]. Overall, the amplitude of the CZ arrivals appears to be an order of magnitude ($\times 10$) louder than receptions made at other locations, i.e., a 20 dB increase in amplitude level, which is consistent with the ray tracing predictions shown in Fig. 2. For completeness, Figs. S3 and S4 show the envelopes of the full recorded waveform from each of the 30 successive WHOI-TR transmissions corresponding to the same ASV locations shown in Fig. 3. Overall, the comparison between the TAM's measurements and the ray tracing simulations shown in Figs. 2 and 3 confirms that the simulated sound speed profiles obtained from the selected regional ocean model and selected bathymetry resolution for the area are sufficiently accurate to predict the dominant features of the low-frequency sound prediction between WHOI-TR and the ASV, such as the occurrence of the CZ (see Figs. S3 and S4) or blockage of the main propagation paths between them by

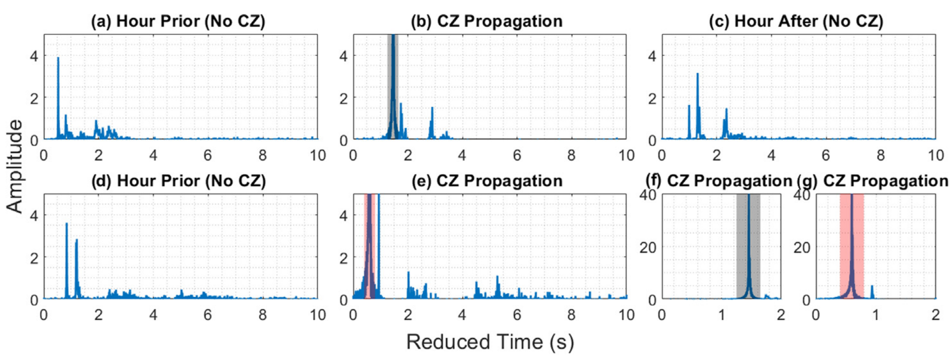

Fig. 3. Mean value of the time-aligned (based on the first arrival wavefront) envelopes recorded across the 30-element synthetic aperture (i.e., incoherent stacking) of the arrival wavefront structure of the hours before and during and the hour after the WG passed the location where the west [(a), (b), and (c)] CZ propagation annulus and the east [(d) and (e)] occur. No data were available for the hour after the WG crossed the eastern CZ annulus. The first arrivals corresponding to CZ propagation in panels (b) and (e) are shown in panels (f) and (g), respectively, with their full amplitude shown. In panels (b) and (f) and (e) and (g), the propagation paths corresponding to CZ propagation are shaded in black and red, respectively.

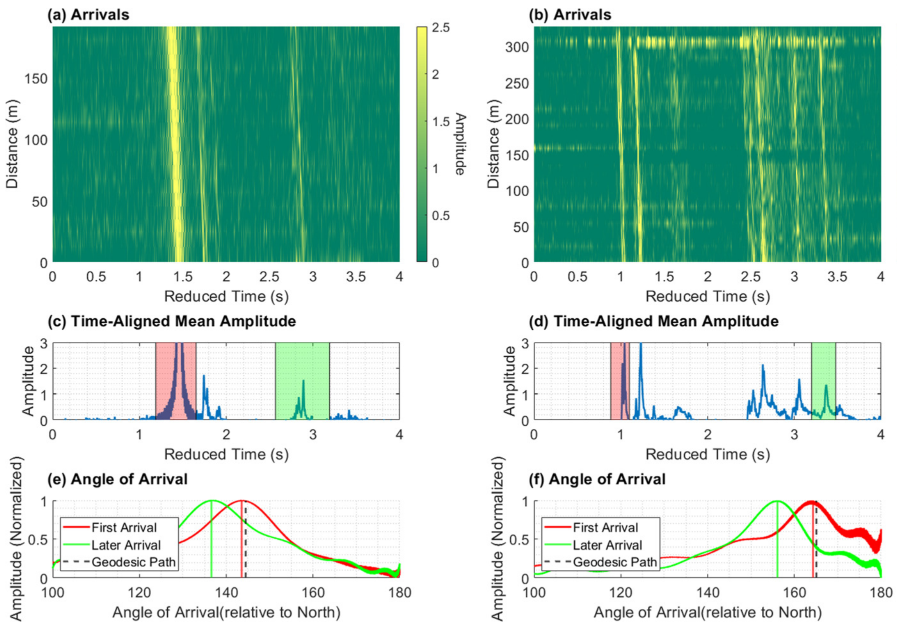

Fig. 4. Arrival-time structure recorded along the 30 WG positions used to create the horizontal synthetic aperture [(a) and (b)], mean value of the time-aligned (based on the first arrival) envelopes recorded on the selected horizontal synthetic aperture [(c) and (d)], and selected plane wave beamformer outputs [(e) and (f)] for two WG locations. For the left column panels, the WG was near where the western CZ arrival from WHOI-TR occurred (same as shown in Fig. 3). For the right column panels, the WG is located above A2 seamounts. Specific locations of the WG overlying the bathymetry are shown in Fig. S6 in the supplementary material.

the Caldera (see Fig. S5). However, as expected, accurate predictions of the weaker reverberation structure visible in the TAM's recordings shown in Fig. 3 (and see Figs. S3–S5) were not found to be possible with the selected modeling approach.

To further investigate the spatial origin of the multipath structure observed on the TAM's recordings, Fig. 4 displays the results of synthetic aperture beamforming processing for two selected locations of the ASV. The left column panels of Fig. 4 correspond to a location (38.4465 N, 63.3782 W) on the western side of the seamounts where the ASV intercepted CZ propagation paths from WHOI-TR, the same location as Figs. 3(b) and 3(f). Beamforming results confirm that the strongest first CZ arrival (red window) occurs along in-plane propagation at an apparent bearing angle of 143.6°, i.e., along the geodesic path linking WHOI-TR and the ASV. Note that the standard deviation of the array heading during the reception period was 0.74°. The effective values for the synthetic aperture and element spacing used to generate the beamforming results in Fig. 4(e) were $L = 191.73$ m and $d = 10.65$ m (see Fig. S2). However, the weaker reverberation arrivals (green window) appear to originate from slightly out-of-plane propagation at an apparent bearing angle of 136.7°, which thus likely results from scattering from the seamount flanks.

On the other hand, the right column panels of Fig. 4 correspond to a location (38.4337 N, 63.1441 W) where the ASV was above the southern edge of the A2 summit and approaching the Caldera seamount. Beamforming results for this configuration also confirm that the first arrivals (red window) occur along in-plane propagation at an apparent bearing angle of 164.3°. Note that the standard deviation of the array heading during the reception period was 2.10°. The effective values for the synthetic aperture and element spacing used to generate the beamforming results in Fig. 4(f) were $L = 327.5$ m and $d = 10.91$ m (see Fig. S2). However, the later multipath arrivals (starting after 2.5 s reduced time) exhibit a highly complex mixture of distinct peaked arrivals surrounded by a more diffuse reverberation structure. Beamforming onto the last peaked arrival (green window) indicates that it is associated with more pronounced out-of-plane propagation at an apparent bearing angle of 156.0°. Similar out-of-plane propagation angles were found for the preceding group of peaked arrivals visible in this later multipath structure. Additionally, given the shallow receiver depth ($\sim$12 m), ocean surface scattering effects will likely also influence the observed scattering effects induced by the seamounts.

4. Conclusions

In this work, we show that an instrumented ASV can be used to characterize the spatial variability of low-frequency deep-water sound propagation. The study area was centered around A2 seamounts, a feature that significantly affected local sound propagation. Notably, it caused blockage of in-plane propagation paths from a bottom-mounted source in-stratum with the SOFAR channel when the shallow ASV's TAM receiver was located behind the Caldera seamount, along with an overall complex reverberation structure, which displayed 3D out-of-plane propagation effects as confirmed by horizontal synthetic aperture beamforming. The TL predictions using the simple modeling approach implemented in this study were found to be sufficiently accurate for predicting the main features of the received waveforms, such as the locations of CZ at the shallow depth of the ASV's TAM as well as locations where blockage of in-plane propagation paths occurs due to the influence of the Caldera seamount. However, the standard modeling approach used in this study did not capture the more complex propagation effects associated with the rough seafloor and seamount scattering. To do so would likely require using full waveform 3D acoustic modeling combined with inputs from high-resolution bathymetry and potentially a higher-resolution ocean model.

Supplementary Material

See the supplementary material for supporting data and a schematic of the synthetic array procedure.

Acknowledgments

The authors acknowledge Evan Harris and Luke Colosi for their assistance with wave glider engineering development and field operations. Thanks to Dr. Y. T. Lin for providing information regarding WHOI-TR source operations. Thanks also to the cruise Chief Scientist, Dr. Matthew Alford, and crew members of R/V *Neil Armstrong* for their cruise support. M.M., D.R., and K.G.S. received funding under Grant No. N00014-24-1-2439 from the Office of Naval Research (ONR). L.G. and L.L. also received funding from ONR under Grant Nos. N00014-23-1-2237, N00014-21-1-2791, and N00014-21-1-2817. G.G. received funding under ONR Grant No. N00014-21-1-2907.

Author Declarations

Conflict of Interest

The authors have no conflicts to disclose.

Data Availability

The data that support the findings of this study are available with the article and its supplementary material. The raw data supporting this study's conclusions are available upon request from K.G.S. The ETOPO-1 database can be found at http://www.ngdc.noaa.gov/mgg/global/global.html. Copernicus Marine Environment Monitoring Service (CMEMS) sea surface height data can be found at https://data.marine.copernicus.eu/product/SEALEVEL_GLO_PHY_L4_NRT_008_046/description. ERA5 reanalysis can be found at http://www.ecmwf.int/en/forecasts/dataset/ecmwf-reanalysis-v5. RADS can be found at http://rads.tudelft.nl/rads/index.shtml. The SST data can be found at https://coastwatch.noaa.gov/cwn/products/noaa-geo-polar-blended-global-sea-surface-temperature-analysis-level-4.html.

References

Autrey, S. W. (**1988**). "Passive synthetic arrays," J. Acoust. Soc. Am. **84**(2), 592–598.

Ballard, M. S., and Sagers, J. D. (**2019**). "Measurements and modeling of acoustic propagation in a scale model canyon," J. Acoust. Soc. Am. **146**(3), 1858–1866.

Ballard, M. S., Sagers, J. D., Poulain, P. M., Mackinnon, J., Lucas, A. J., and Sanchez-Rios, A. (**2023**). "Out-of-plane arrivals recorded by drifting hydrophones during the Northern Ocean Rapid Surface Evolution Experiment," J. Acoust. Soc. Am. **154**(5), 2757–2768.

Chassignet, E. P., Hurlburt, H. E., Smedstad, O. M., Halliwell, G. R., Hogan, P. J., Wallcraft, A. J., Baraille, R., and Bleck, R. (**2007**). "The HYCOM (HYbrid Coordinate Ocean Model) data assimilative system," J. Mar. Syst. **65**(1–4), 60–83.

Forget, G., Campin, J.-M., Heimbach, P., Hill, C. N., Ponte, R. M., and Wunsch, C. (**2015**). "ECCO version 4: An integrated framework for non-linear inverse modeling and global ocean state estimation," Geosci. Model Dev. **8**(10), 3071–3104.

Godin, O. A., Tan, T. W., Joseph, J. E., and Walters, M. W. (**2024**). "Observation of exceptionally strong near-bottom flows over the Atlantis II Seamounts in the Northwest Atlantic," Sci. Rep. **14**(1), 10308.

Grare, L., Statom, N. M., Pizzo, N., and Lenain, L. (**2021**). "Instrumented wave gliders for air-sea interaction and upper ocean research," Front. Mar. Sci. **8**, 664728.

Guo, Y., Duan, R., Zhang, H., Yang, K., Liu, T., and Gong, G. (**2023**). "Modeling and interpretation of bistatic bottom reverberation in deep water near seamounts," J. Acoust. Soc. Am. **154**(5), 3173–3187.

Heaney, K. D., and Baggeroer, A. B. (**2006**). "Measurements of 3-dimensional downslope acoustic propagation during the Basin Acoustic Seamount Scattering EXperiment (BASSEX-04)," in *OCEANS 2006—Asia Pacific*, Singapore (IEEE, New York), pp. 1–6.

Jensen, F. B., Kuperman, W. A., Porter, M. B., and Schmidt, H. (**2011**). *Computational Ocean Acoustics*, 2nd ed., Modern Acoustics and Signal Processing (Springer, New York).

Johnson, D. H., and Dudgeon, D. E. (**1993**). *Array Signal Processing: Concepts and Techniques* (Prentice Hall, Upper Saddle River, NJ).

Lin, Y. T., Duda, T. F., and Newhall, A. E. (**2013**). "Three-dimensional sound propagation models using the parabolic-equation approximation and the split-step Fourier method," J. Comput. Acoust. **21**(01), 1250018.

Lin, Y. T., Van Uffelen, L. J., Miller, J. H., Potty, G. R., and Vigness-Raposa, K. J. (**2022**). "Horizontal refraction and diffraction of underwater sound around an island," J. Acoust. Soc. Am. **151**(3), 1684–1694.

Luo, W., and Schmidt, H. (**2009**). "Three-dimensional propagation and scattering around a conical seamount," J. Acoust. Soc. Am. **125**(1), 52–65.

Mallik, W., Jaiman, R., and Jelovica, J. (**2024**). "Deep neural network for learning wave scattering and interference of underwater acoustics," Phys. Fluids **36**(1), 017137.

Marshall, J., Adcroft, A., Hill, C., Perelman, L., and Heisey, C. (**1997**). "A finite-volume, incompressible Navier Stokes model for studies of the ocean on parallel computers," J. Geophys. Res., [Oceans] **102**(C3), 5753–5766, https://doi.org/10.1029/96JC02775.

McKinley, M., Sun, D., Kelly, M., Sabra, K. G., and Bracco, A. (**2024**). "Deep mesoscale and submesoscale circulations around the Atlantis II seamount," J. Geophys. Res., [Oceans] **129**(11), e2024JC021233, https://doi.org/10.1029/2024JC021233.

National Oceanic and Atmospheric Administration (**2024a**). "Radar Altimeter Database System (RADS)," https://www.star.nesdis.noaa.gov/socd/lsa/RADS.php (Last viewed 2024).

National Oceanic and Atmospheric Administration (**2024b**). "NOAA geo-polar blended global sea surface temperature analysis (level 4)," https://coastwatch.noaa.gov/cwn/products/noaa-geo-polar-blended-global-sea-surface-temperature-analysis-level-4.html (Last viewed 2024).

Porter, M. B. (**2011**). "The Bellhop manual and user's guide: Preliminary draft," Technical Report 260 (Heat, Light, and Sound Research, Inc., La Jolla, CA).

Porter, M. B. (**2019**). "Beam tracing for two- and three-dimensional problems in ocean acoustics," J. Acoust. Soc. Am. **146**(3), 2016–2029.

Premus, V. E., Abbot, P. A., Kmelnitsky, V., Gedney, C. J., and Abbot, T. A. (**2022**). "A wave glider based, towed hydrophone array system for autonomous, real-time, passive acoustic marine mammal monitoring," J. Acoust. Soc. Am. **152**(3), 1814–1828.

Roquet, F., Madec, G., McDougall, T. J., and Barker, P. M. (**2015**). "Accurate polynomial expressions for the density and specific volume of seawater using the TEOS-10 standard," Ocean Modell. **90**, 29–43.

Stammer, D., Wunsch, C., Giering, R., Eckert, C., Heimbach, P., Marotzke, J., Adcroft, A., Hill, C. N., and Marshall, J. (**2002**). "Global ocean circulation during 1992–1997, estimated from ocean observations and a general circulation model," J. Geophys. Res., [Oceans] **107**(C9), 1-1–1-27, https://doi.org/10.1029/2001JC000888.

Treloar, A. A., Maclean, H., Bujalka, J., Narramore, J., Thomas, B., Blondel, P., and Hunter, A. (**2024**). "Real-time in-situ passive acoustic array beamforming from the AutoNaut wave-propelled uncrewed surface vessel," IEEE J. Ocean. Eng. **49**, 713–726.

Walters, M. W., Godin, O. A., Joseph, J. E., and Tan, T. W. (**2024**). "Deep-water ambient sound over the Atlantis II seamounts in the Northwest Atlantic," J. Acoust. Soc. Am. **156**(4), 2687–2700.